Thermodynamic Modelling of the U-Dy-O System

S. White, B.J. Lewis and W.T. Thompson*
Department of Chemistry and Chemical Engineering, Royal Military College of Canada,
Kingston, Ontario K7K 7B4
**corresponding author <thompson-w@rmc.ca>*

Sven C. Vogel
Lujan Neutron Scattering Center, Los Alamos National Laboratory, Los Alamos, NM

ABSTRACT

Among the important fission products dissolved in UO_2 are several members of the lanthanide series. Particular lanthanide sesquioxides (Ln_2O_3), notably Dy_2O_3, are of interest as burnable neutron poisons in advanced CANDU fuel bundle designs. For these reasons, a systematic evaluation of the existing thermodynamic knowledge of known UO_2 - Ln_2O_3 systems is being undertaken. A proposed binary phase diagram for UO_2-Dy_2O_3 is based on the generally similar chemical behaviour of all Ln_2O_3 as well as Y_2O_3 systems involving UO_2.

Uranium and lanthanide oxides form rhombohedral compounds of the form ULn_6O_{12} under oxidizing conditions. The significance in understanding the phase equilibrium in the ternary U-Dy-O system at 1600°C will be discussed. Computed phase diagrams, based on some estimated data, draw attention to the potential importance of oxygen partial pressure. The computed diagrams provide the rationale for sample preparation in ongoing experimental studies.

1. INTRODUCTION

Phase equilibrium in the UO_2-Dy_2O_3 system bears upon the manufacture and performance of fuel in an advanced CANDU bundle design[1,2]. In this developing technology, slightly isotopically-enriched UO_2 (SEU) outer fuel elements surround a central element containing, in addition to UO_2, a significant dissolved concentration of Dy, a burnable neutron poison.

In principle, all lanthanide (or rare earth; atomic numbers 57-71) sesquioxides, collectively represented by the formula Ln_2O_3, are soluble to a considerable degree in UO_2 (3) and several of these are significant fission products that accumulate normally in CANDU fuel during burnup. When exposed to even slightly oxidizing conditions, mixtures of UO_2 and Ln_2O_3-type oxides form a rhombohedral phase with the formulation ULn_6O_{12}[4-7]. The conditions under which this phase may develop are of interest especially when the concentration of Ln_2O_3 is as high as proposed in doped fuel (Ln=Dy^{66}). This matter may have a bearing on sintering technology to produce the doped fuel pellets. Moreover the potential formation of this phase by D_2O in a fuel element that develops a sheathing breach may influence the in-reactor oxidation behaviour. For these reasons, it is helpful to have phase diagrams for the U-Dy-O system spanning a wide range of oxygen partial pressure.

Relatively little information on the U-Dy-O phase equilibrium is available. Fortunately, all the lanthanides and Y (which has the same outer electron configuration as La with comparable atomic radius) behave in a chemically similar way. Thus, it is possible to estimate with some confidence the chemical properties of one Ln-containing compound or phase from those of the others.

2. ESTIMATED UO_2-Dy_2O_3 BINARY PHASE DIAGRAM

Pure Dy_2O_3 exists in three crystal structures[8]. The cubic modification existing from room temperature to 1807°C is structurally very similar to UO_2. The arrangements of oxide and metal ion sites in both UO_2 and cubic Dy_2O_3 are isomorphous with CaF_2 (fluorite). In UO_2, all anion sites are occupied with O^{2-}; in Dy_2O_3 however, one fourth of the oxide ions sites are vacant in a regular three dimensional pattern leading to the assignment of a different space group classification for Dy_2O_3 (Ia3) and UO_2 (Fm3m). In recognizing this structural similarity, the formula mass for Dy_2O_3 is sometimes written as $DyO_{1.5}$. This similarity makes possible in principle a continuous cubic solid solution from pure UO_2 to pure $DyO_{1.5}$, although the crystal structures for the component oxides are classified differently. The solid solution is a near random mixing of U^{4+} and Dy^{3+} ions on the cation sites surrounded by a cubic cage of oxide ions with a progressively increasing fraction of vacancies as the Dy^{3+} concentration increases; half of oxide ion cubic cages are vacant of any cations. The thermodynamic description of such a common anion phase can be formulated with a mixing term based on the random mixing of cations and an excess function. Following the general appearance of the chemically similar UO_2-Y_2O_3 system[3] shown in Figure 1, the form of this excess term for the cubic solid solution of UO_2 and Dy_2O_3 was taken to be

$$G^E = p \; X_{UO2} \; X_{Dy2O3}{}^3$$

The choice of this formulation, and the power on X_{Dy2O3} in particular, is essentially empirical and made as simple as possible to provide for a skewed miscibility gap as in the UO_2-Y_2O_3 system using only one adjustable parameter.

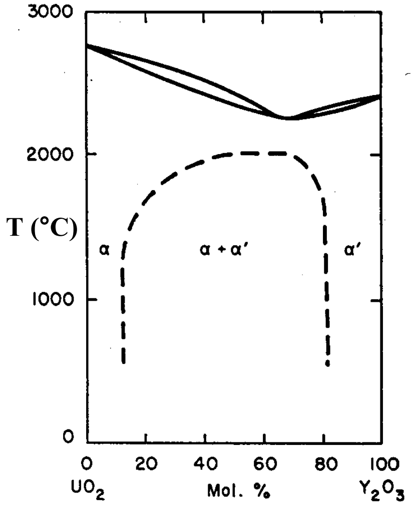

Figure 1. UO_2-Y_2O_3 Phase Diagram Showing Skewed Miscibility Gap[3]

With the parameter p selected as +42000 J/mol, Gibbs energy curves for the UO_2-Dy_2O_3 system are shown in Figure 2 at 1000°C and 2000°C.

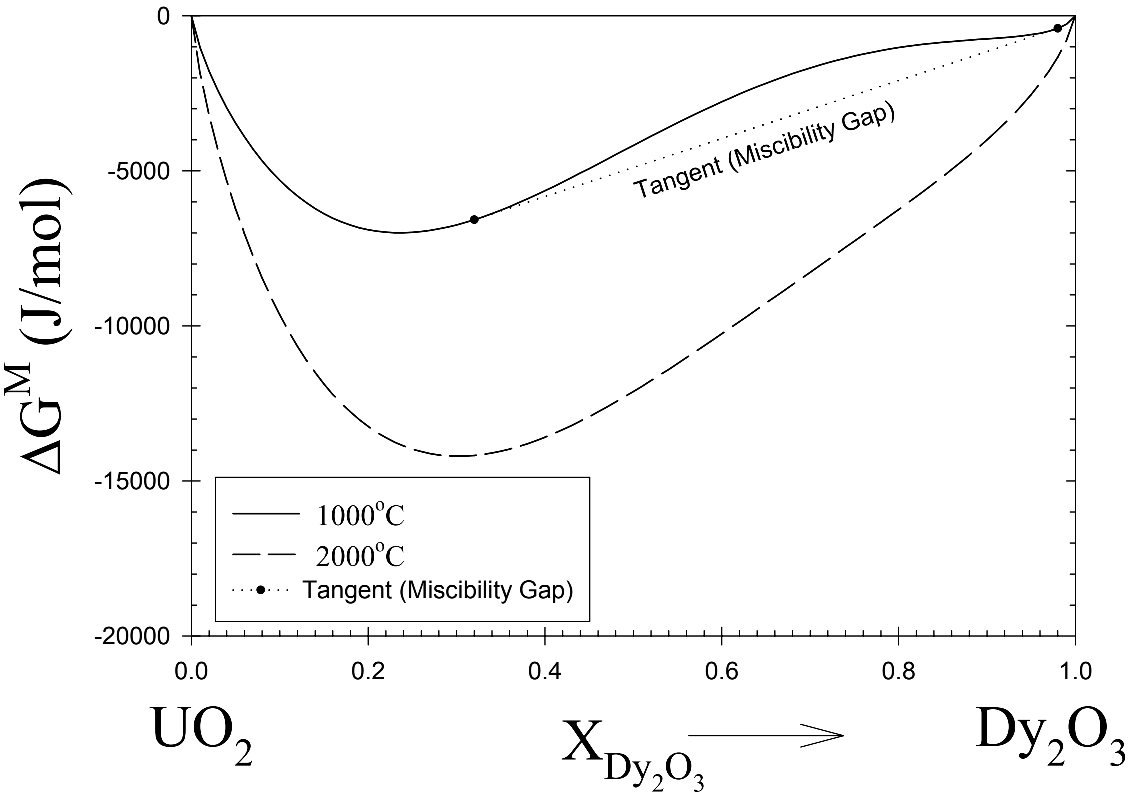

Figure 2. Estimated Gibbs Energy Curves for UO_2-Dy_2O_3 Solid Solution Based on Behaviour that is Expected to be Similar to UO_2-Y_2O_3

At the upper temperature, the dashed curve is concave over the extremes of composition; therefore, a solid solution is continuous from the extremes of composition. At the lower temperature, the greater relative influence of the proposed excess Gibbs energy term over the ideal ion mixing term creates points of inflection. The common tangent construction to this curve identifies the compositions of coexistent solid solutions provided by the estimate of parameter p[9]. The Gibbs energy of this two-phase mixture (with compositions given by the line between the points of tangency) is slightly lower than a one-phase solid solution. This small Gibbs energy difference is the driving force for spinodal phase decomposition. This concept is the basis for constructing the placement of the miscibility gap in the cubic solid solution for the proposed UO_2-Dy_2O_3 phase diagram in Figure 3. The same concept generates the other features of the diagram. For the case of the liquid phase, there is of course another Gibbs energy curve involving the Gibbs energy change for component melting. This is illustrated in Figure 4. For the liquid phase, the excess mixing term was set to zero. The proposed UO_2-Dy_2O_3 system bears the intended resemblance to the chemically similar UO_2-Y_2O_3 system in Figure 1 which inspired the above mentioned treatment and, in particular, the selection of the form of excess Gibbs energy term as well as the estimated value of parameter p. No evidence is offered here in support of the diagram in Figure 3, but it is the basis for selecting temperatures and compositions for ongoing experimental work to better locate the placement of the miscibility gap and the melting point suppression of UO_2 by Dy_2O_3.

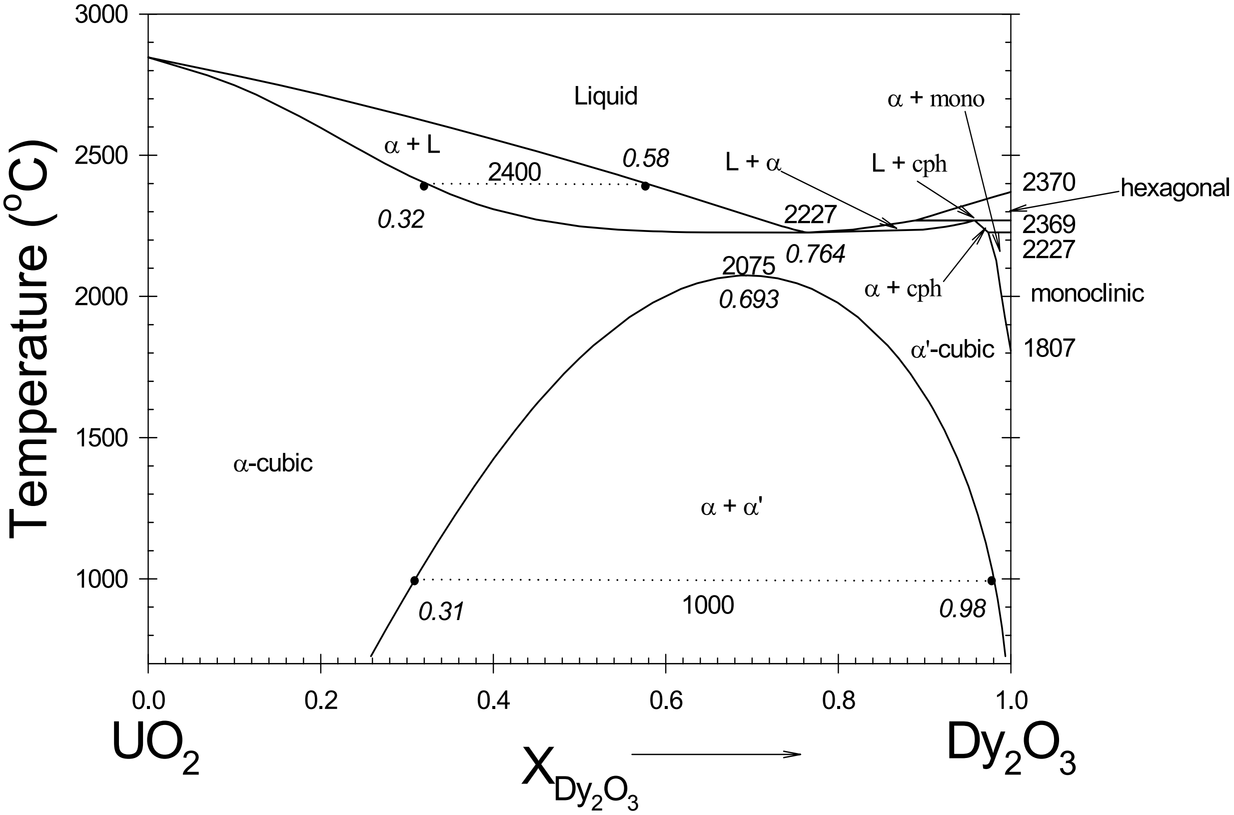

Figure 3. Estimated UO_2-Dy_2O_3 Phase Diagram Based on Expected Similarity to Figure 1

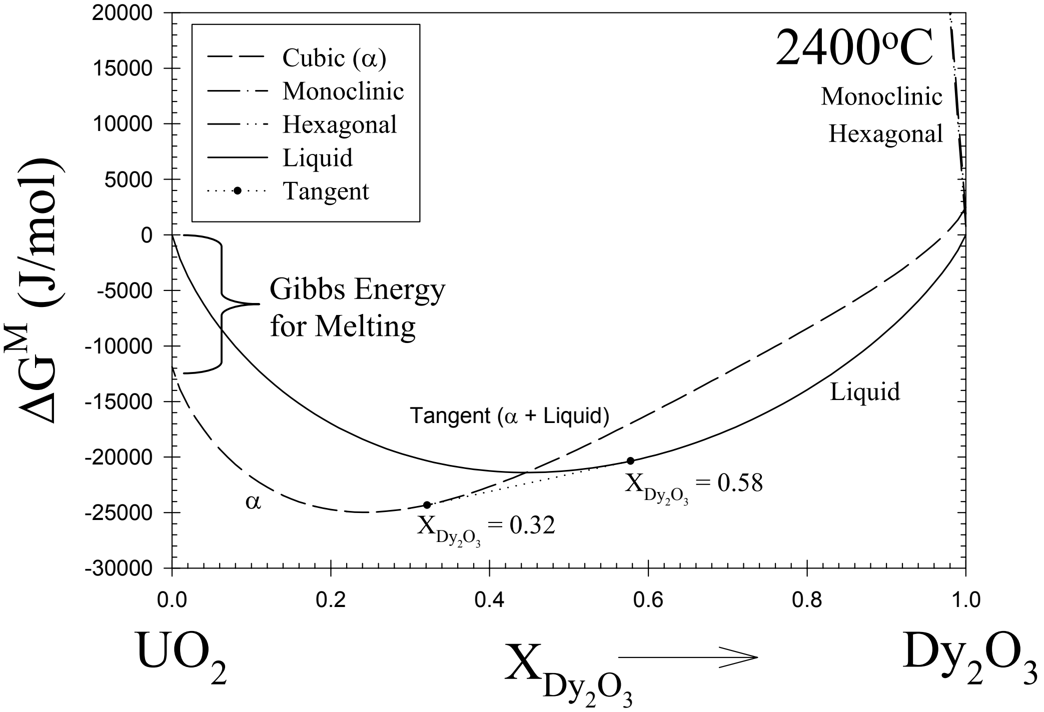

Figure 4. **Gibbs Energy Curves for UO_2-Dy_2O_3 Solid and Liquid Phases at 2400°C**

3. ESTIMATED TERNARY U-Dy-O PHASE DIAGRAMS

Several publications have established conclusively the existence and crystal structure of compounds of the type ULn_6O_{12} [4-7.] These have been reported for every lanthanide except Er. The structure for ULa_6O_{12} is shown in Figure 5 from the work of Hinatsu[5].

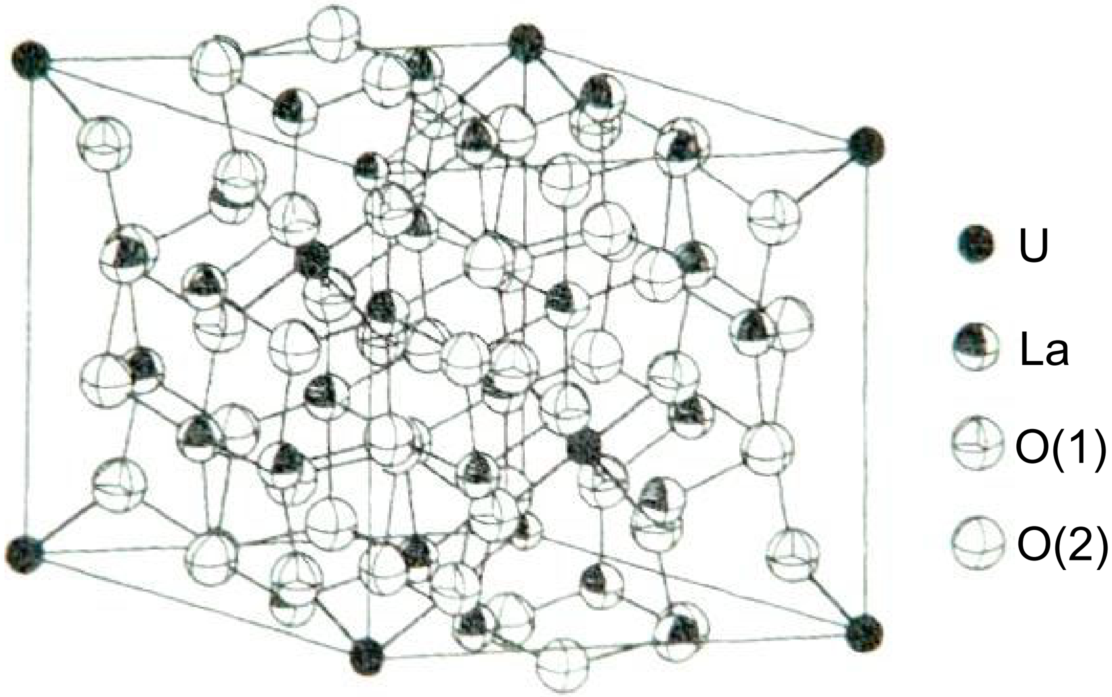

Figure 5. **Crystal Structure of ULa_6O_{12}[5]**

These compounds may be prepared in the laboratory by heating uranium and lanthanide oxide mixtures in the presence of air[5,6]. The source of the oxygen need not necessarily be air but, more to the point, the partial pressure of oxygen sufficient to cause the reaction need not be great. In the applications under discussion, the oxygen could be provided by H_2O in a sufficiently humidified mixture with H_2 as in sintering fuel pellets, via the gas phase equilibrium

$$2\,H_2 + O_2 = 2\,H_2O \qquad \textbf{(1)}$$

Alternately, the source of oxygen could be associated with hyperstoichiometry of UO_2 with an O/U ratio greater than 2 otherwise written as (UO_{2+x}).

In a defected fuel element, UO_{2+x} arises by reaction of the heavy water coolant with the initially near-stoichiometric UO_2

$$UO_2 + x\,D_2O \rightarrow UO_{2+x} + x\,D_2 \qquad \textbf{(2)}$$

Since the hyperstoichiometric fuel composition can otherwise be expressed as dissolved UO_3

$$UO_{2+x} = \{ (1-x)\, UO_2 + x\, UO_3 \} \qquad \textbf{(3)}$$

UDy_6O_{12} could arise by the reaction

$$(UO_3)_{\text{dissolved in UO2}} + 3\,(Dy_2O_{3+})_{\text{dissolved in UO2}} \equiv UDy_6O_{12} \qquad \textbf{(4)}$$

when the combination of concentrations of UO_3 (degree of hyperstoichiometry, x, in UO_{2+x}) and Dy_2O_3 are high enough (that is, exceeds a temperature-dependent solubility product).

The requirement for oxygen in excess of that provided by a mixture of only UO_2 and Dy_2O_3 implies that UDy_6O_{12} (otherwise written as $UO_3.(Dy_2O_3)_3$) cannot be expected in the UO_2-Dy_2O_3 binary phase diagram. UDy_6O_{12} lies out of the plane of this diagram. This matter is made clearer in Figure 6 which places UDy_6O_{12} on the join connecting UO_3 and Dy_2O_3.

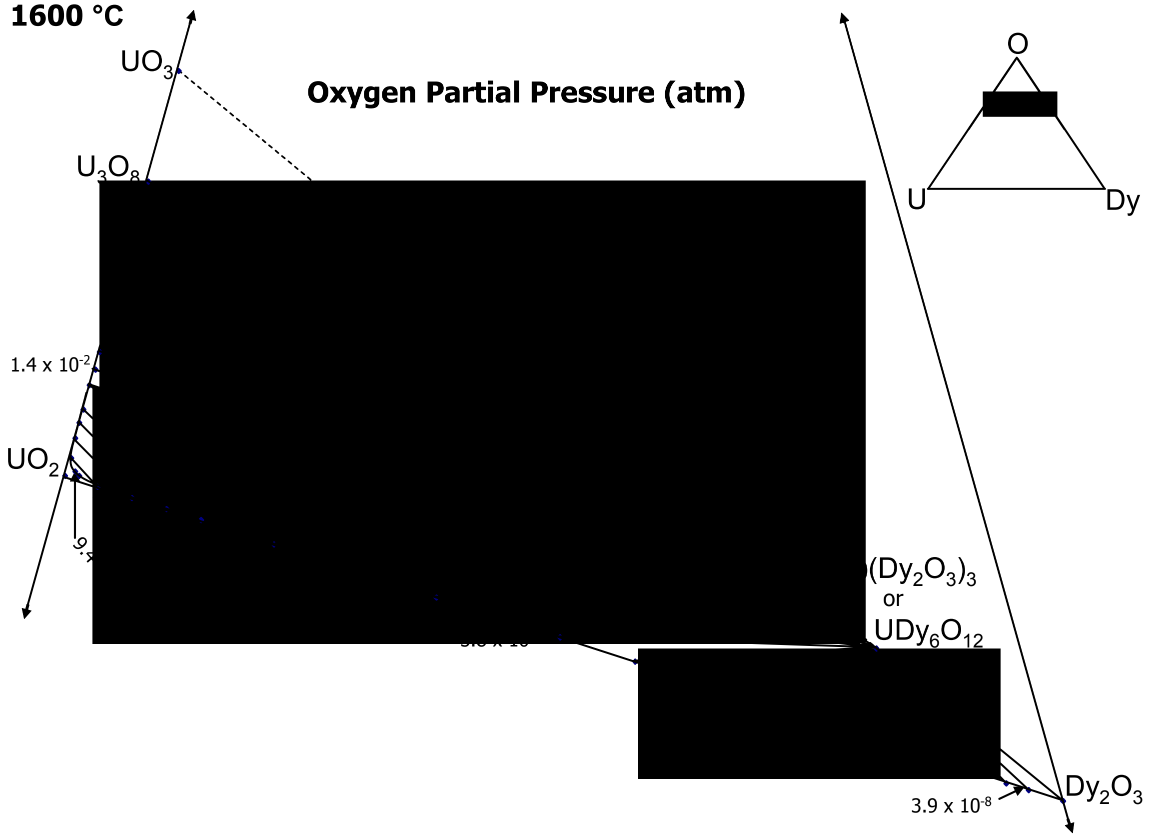

[redacted]

[redacted]

[redacted]

Figure 6. Distorted Section of Proposed U-Dy-O Phase Diagram with Oxygen Partial Pressures

From the vapour pressure measurements of Aitken[4], the Gibbs energy of formation of UDy_6O_{12} from UO_3 vapour and Dy_2O_3 solid can be calculated. This data combined with a treatment for UO_{2+x} and the estimated behaviour for Dy_2O_3 dissolved in UO_2 (described above), makes possible the calculation of the partial pressure of oxygen gas sufficient to provide the degree of hyperstoichiometry in UO_{2+x} required for dissolved Dy_2O_3 to react to form UDy_6O_{12}. The pressures associated with phase coexistence in Figure 6 clearly show that even quite low partial oxygen pressures are sufficient to cause the appearance of UDy_6O_{12} *when the concentration of* Dy_2O_3 *dissolved in the* UO_2 *is high enough*. The placement of the rhombohedral phase on Figure 6 is consistent with a previously published diagram at 1250°C[10]. The diagram in Figure 6 may be reconstructed in a more useful way for the present purpose by placing log P_{O2} as ordinate on an isothermal diagram with the metal atom fraction Dy as the abscissa [11]. This provides the phase diagram in Figure 7 with the same recognizable topology as Figure 3 but puts emphasis on the importance of partial oxygen pressure on the phase equilibrium in the U-Dy-O system. In the context of nuclear fuel manufacture and operation, it is useful to show in Figure 7 H_2/H_2O mixtures that generate the corresponding oxygen partial pressure via the equilibrium in reaction (1). This is shown by the right hand scale. It should be noted that the oxygen partial pressure depends only on the H_2O/H_2 ratio and is independent of the total gas pressure.

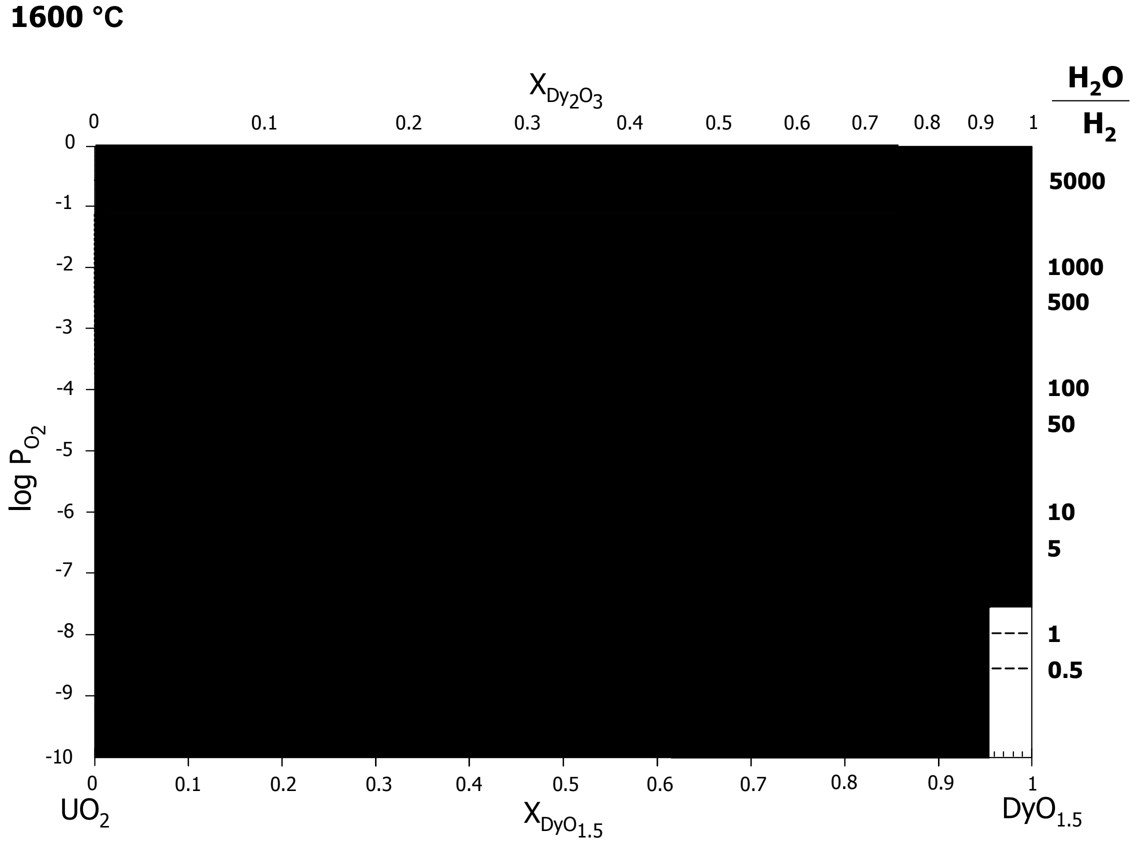

Figure 7. UO_2-$DyO_{1.5}$ Phase Diagram with logP_{O2} as Ordinate and Metal-Fraction Dy as Abscissa (equivalent to mole fraction of $DyO_{1.5}$ shown). The scale on the top of the diagram converts the mole fraction of $DyO_{1.5}$ into the equivalent expressed in terms of Dy_2O_3.

A particularly noteworthy, and questionable, feature of the proposed diagram in Figure 7 is the two cubic phase region associated with the spinodal decomposition of the intended fuel phase. This arises as a consequence of the interpolation procedure used to generate the Gibbs energy for this phase[12]. In the subsequent processing to develop the likely phase boundaries by Gibbs energy minimization, two fluorite phases with different compositions are found to be more stable than one. The implications are that a one-phase solid solution of UO_2 and Dy_2O_3 rich in U may, under slightly oxidizing conditions, spontaneously decompose into two cubic solid solutions: one that could be described as approximately $(U^{4+},U^{6+})O_{2+x}$ and another described as $(U^{4+},Dy^{3+})O_{2-z}$.

4. EXPERIMENTAL VERIFICATION

The diagrams in Figures 6 and 7 are to be understood as *provisional since they are based entirely on computation using some data that is estimated*. Nonetheless, the diagrams do provide a rationale for the selection of sample preparation conditions preliminary to phase identification planned by neutron diffraction. Since Dy is a strong neutron absorber, preliminary tests have been conducted on mechanical mixtures of UO_2 and Dy_2O_3 to confirm that phase proportions can be extracted by Rietveld refinement. Powdered samples involving mixtures of slightly hyperstoichiometric UO_2 with 10 weight percent Dy_2O_3 sealed in evacuated quartz containers were studied at the Los Alamos Neutron Science Center at room temperature. These studies returned phase proportions by Rietveld refinement of $UO_{2.1}$ and Dy_2O_3 in the range 9.5 to 13 weight percent at 3, 10, and 60 minute exposure times. These results are sufficiently encouraging to plan additional beam studies on sample mixtures sintered under controlled conditions. This is expected to not only provide the basis for revising phase diagrams of the type shown in Figure 6 and 7 but should also provide thermodynamic properties useful in other thermochemical computations of significance to the Dy-doped fuel program.

5. CONCLUSIONS

Computed phase diagrams are proposed for the U-Dy-O system based in part on estimated data. These diagrams draw attention to the importance of including the oxygen partial pressure as an important variable. The diagrams are providing the basis for sample preparation conditions at Cameco preliminary to neutron beam studies at the Los Alamos Neutron Science Centre.

6. ACKNOWLEDGEMENTS

The authors thank Cameco Corporation, in particular Dr. Simon Reid, for samples of UO_2-Dy_2O_3 mixtures prepared and sent to the Los Alamos Neutron Science Centre. They thank M.H. Kaye for assistance in preparing Figure 6 and F. Akbari for helpful discussions. The financial assistance of the Natural Sciences and Engineering Research Council of Canada in the form of a Discovery Grant (WTT) is also gratefully acknowledged.

REFERENCES

1. P. Boczar, “Advanced Fuel Development in AECL,” *Canadian Nuclear Society Bulletin*, **24** [4] (December 2003), 17. (presented at the 8th International Conference on CANDU Fuel, Honey Harbour, Ontario, September 21-24, 2003).
2. M. Liska and D. McArthur, “Bruce Power New Fuel Project, Design and Implementation of Bruce CANFLEX-L VRF,” *Canadian Nuclear Society Bulletin*, **24** [4] (December 2003), 26. (presented at the 8th International Conference on CANDU Fuel, Honey Harbour, Ontario, September 21-24, 2003).
3. ACers-NIST Phase Equilibria Diagrams, Version 3.0, American Ceramic Society and National Institute of Standards and Technology, (2004).
4. E. A. Aitken, S. F. Bartram, and E. F. Juenke, “Crystal Chemistry of the Rohombohedral $MO_3.3R_2O_3$ Compounds”, *Inorg. Chem*., **3** (1964), 949-953.
5. Y. Hinatsu, N. Masaki, and T. Jujino, “The Crystal Structure of La_6UO_{12}”, *J. Solid State Chem.*, **73** (1988), 567-571.
6. Jena Hrudananda, R. Asuvathraman, M. V. Krishnaiah, and K. V. Govindan Kutty, “X-ray powder diffraction of RE_6UO_{12} (RE=Eu, Gd, and Dy)”, *Powder Diffraction*, **16** (4) (2001), 220-223.
7. M. V. Krishnaiah, G. Seenivasan, P. Srirama Murti, C. K. Mathews, “Thermal conductivity of rare earth–uranium ternary oxides of the type RE_6UO_{12}”, *Journal of Nuclear Materials*, **306** (2002), 10–14.
8. G. Adachi, N. Imanka, and Z.C. Kang, eds., <u>Binary Rare Earth Oxides</u>, Dordrecht: Kluwer Academic Publishers, (2004).
9. M. H. Kaye, K. M. Jaansalu, and W. T. Thompson, “Phase Equilibrium in Metallic Systems”, *Canadian Metallurgical Quarterly*, **42** (4) (2003), 393-410.
10. I. B. DeAlleluia, M. Hoshi, W. G. Jocher, and C. Keller, “Phase Relationships for the Ternary UO_2-UO_2-$REO_{1.5}$ (RE = Rr, Nd, Dy) Systems”, *Journal of Inorganic Nuclear Chemistry*, **43** [8] (1981), 1831-1834.
11. A.D. Pelton and W.T. Thompson, “Phase Diagrams”, *Progress in Solid State Chemistry*, **10** [3] (1975), 119-155.
12. F. Kohler, *Monats. Chem.*, **91** (1960), 738-740.